Resonances in $\bar{p}p \to \eta\pi^+\pi^-\pi^+\pi^-$ at rest

A.V. Anisovich [b], D.V. Bugg [c], N. Djaoshvili [a], C. Hodd [c],
L. Montanet [a], A.V. Sarantsev [b], B.S. Zou [c,1]

[a] *CERN, CH-1211 Geneva 4, Switzerland*

[b] *St. Petersburg Nuclear Physics Institute, Gatchina, St. Peterburg district, Russia 199350*

[c] *Queen Mary and Westfield College, London E1 4NS, UK*

PACS: 13.75Cs, 14.20GK, 14.40
Keywords: mesons, resonances, annihilation

Abstract

Data on $\bar{p}p \to \eta\pi^+\pi^-\pi^+\pi^-$ at rest show two resonant processes: (a) $f_0(1370)\eta$, $f_0(1370) \to \sigma\sigma$ and $\rho\rho$, (b) $\eta(1440)\sigma$, $\eta(1440) \to \eta\pi^+\pi^-$. The branching ratio $BR[f_0(1370) \to \rho\rho]/BR[f_0(1370) \to \sigma\sigma] = 0.98 \pm 0.25$ in the mass range available here. Using data on $\bar{p}p \to \eta\pi^0\pi^0$, the ratio $\Gamma_{4\pi}/\Gamma_{2\pi} \geq 5$ for $f_0(1370)$. The effects of the strongly s-dependent width of $f_0(1370)$ are discussed in some detail.

The $\eta(1440)$ is observed decaying to $\eta\sigma$ and $a_0(980)\pi$, with strong destructive interference between them. In its decay to $a_0(980)\pi$, a narrow peak appears in the $\eta\pi$ mass spectrum, but 30–50 MeV above that usually attributed to $a_0(980)$ and significantly above the KK threshold. This effect is explained naturally by a two-step process: $\eta(1440) \to K^*(890)K$ followed by rescattering of the two kaons through $a_0(980)$ to $\eta\pi$ above the KK threshold.

[1] Now at the Institute for High Energy Physics, Beijing 100039, China

1 Introduction

The first evidence for the E-meson, a pseudoscalar with mass ~ 1425 MeV/c^2, came from the CERN-Collège de France experiment [1] on $\bar{p}p \to K\bar{K}\pi\pi\pi$ at rest. Later a resonance was observed in J/Ψ radiative decays [2] with the same quantum numbers and similar mass and width. This made it a glueball candidate. Evidence for it from the Crystal Barrel experiment has been reported in $\bar{p}p \to \eta\pi^+\pi^-\pi^0\pi^0$ at rest [3] and also in $\bar{p}p \to \eta\pi^0\pi^0\pi^0$ at rest [4]. Many further observations are listed by the Particle Group (PDG) [5], who denote it $\eta(1440)$. There are many surviving puzzles and conflicts, some of which can be addressed with the present data on $\bar{p}p \to \eta\pi^+\pi^-\pi^+\pi^-$ at rest; these data were taken by the Crystal Barrel collaboration at LEAR.

In the present data, a second dominant final state is $f_0(1370)\eta$, $f_0 \to 4\pi$. The $f_0(1370)$ has proved an elusive resonance. The earliest evidence for it came from a weak peak at ~ 1300 MeV in $\pi\pi \to KK$, studied by groups at ANL and BNL [6,7,8]. Because it lies close to the $f_2(1270)$, its status was questionable for many years. It did not appear in CERN-Munich data [9] and this gave rise to doubts about its existence. Fresh evidence for it appeared from Crystal Barrel data on $\bar{p}p \to \eta\eta\pi^0$ [10] and $\bar{p}p \to 3\pi^0$ [11]. In these data, the $f_2(1270)\pi$ channel is suppressed strongly by the $L = 2$ centrifugal barrier for production from the initial $^1S_0$ state; as a result, the $f_0(1370)$ makes a highly significant contribution, though still only 10% of the data.

Evidence for the $f_0(1370)$ has appeared in a number of further experiments. Table 1 summarises results relevant to the present discussion of 4π decays for both $f_0(1370)$ and $f_0(1500)$. The latter is well established, with relative decay rates to 2π and 4π in the range $1 : (1.5 - 2.0)$ [12,13]; it decays strongly to $\sigma\sigma$ and there is little evidence for decays to $\rho\rho$ [22,13]. We shall show here that $\Gamma_{4\pi}/\Gamma_{2\pi} \geq 5$ for $f_0(1370)$. Its absence from CERN-Munich data may be understood from its weak decay to 2π, since its intensity in $\pi\pi \to \pi\pi$ is proportional to $(\Gamma_{2\pi}/\Gamma_{total})^2$. Its intensity in $\bar{p}p$ annihilation is proportional to the first power of $\Gamma_{2\pi}/\Gamma_{total}$ and the square of the coupling constant of $\bar{p}p$ to $f_0(1370)\eta$.

In the mass range around $f_0(1370)$, there is also a very broad state ($\Gamma \sim 1$ GeV) denoted by the PDG as $f_0(400 - 1200)$. Analysis of CERN-Munich and other data [9,12] shows that it couples dominantly to 2π; up to 1330 MeV, the mass range available here, $\Gamma_{2\pi}/\Gamma_{total} \geq 0.85$, see Fig. 4(a) of Ref. [12]. The large $f_0 \to 4\pi$ signal observed here is not compatible with production via $f_0(400 - 1200)$.

The fact that $f_0(1370)$ couples dominantly to 4π raises the question of how to treat its width, which is strongly s-dependent because of the rapid opening

Mass (MeV)	Width (MeV)	Decays	Reference
1410	90	$\rho\rho$	Bettini et al. [14]
1374 ± 38	375 ± 61	$\rho^+\rho^-$, $\sigma\sigma$	Amsler et al. [15]
1386 ± 30	310 ± 50	4π	Gaspero [16]
1345 ± 12	398 ± 26	$\rho\rho$, $\sigma\sigma$	Adamo et al. [17]
1280 ± 55	323 ± 131	$\rho\rho$	Bertin et al. [18]
1370	300	$\rho\rho$, $\sigma\sigma$	Thoma [13]
1306 ± 18	222 ± 46	$\pi\pi$	Barberis et al. [19]
1309 ± 24	226 ± 52	$\pi^+\pi^-\pi^0\pi^0$	Barberis et al. [20]
1295 ± 24	338 ± 52	$\pi^+\pi^-\pi^+\pi^-$	Barberis et al. [20]
1390 ± 30	280 ± 80	$\pi\pi$, $\eta\eta$, $\eta\eta'$	Amsler et al. [21]
1300 ± 15	230 ± 15	$\pi\pi$, $\eta\eta$, $\eta\eta'$	Abele et al. [22]
1505	148	$\sigma\sigma >> \rho\rho$	Bugg et al. [23]
1500	150	$\sigma\sigma$	Abele et al. [24]
1480	130	$\sigma\sigma$	Thoma [13]

Table 1
Summary of masses, widths and decay modes of f_0 resonances relevant to the 4π channel.

of the 4π threshold to $\sigma\sigma$ and $\rho\rho$. This is one of the topics explored here in depth. In most earlier work, it has been fitted with a Breit-Wigner amplitude of constant width. As Achasov and Shestakov have emphasised [25], the effect of the rapidly rising phase space for 4π makes the peak appear in this channel at higher mass than for 2π. We shall show that modelling the s-dependence of the 4π width leads naturally to a difference in these peak positions of 50–100 MeV. This shift between peaks in 2π and 4π helps explain inconsistencies in mass observed in previous publications.

For decays of $\eta(1440)$ to $\eta\pi\pi$, the present data allow a study of its Dalitz plot. This plot has several peculiar features which may have obscured earlier analyses. A narrow peak appears in the $\eta\pi$ mass spectrum, but lies 30–50 MeV above the mass usually attributed to $a_0(980)$ and significantly above the KK threshold. This feature may be explained naturally as the result of rescattering amongst the decay products. From data of BES [26], Mark III [27] and DM2 [28], there is evidence for strong decays of $\eta(1440)$ to K^*K and to a lesser extent to K_0K, where K_0 stands for the $K\pi$ S-wave. Rescattering of the two kaons in the final state through $a_0(980)$ leads to a strong $a_0(980)$ signal which appears in $\eta\pi$, but with the peak displaced above the KK threshold.

The layout of this paper is as follows. Section 2 describes the experimental set-up and the treatment of data. Section 3 discusses the components which are required in the amplitude analysis and discusses branching fractions. Section 4 reviews the treatment of the s-dependent width of $f_0(1370)$. Section 5 discusses the $\eta(1440)$ and the effect of triangle diagrams in its decay. Section 6 summarises conclusions.

2 Experiment and Data Processing

The data reported here on $\bar{p}p \to \eta\pi^+\pi^-\pi^+\pi^-$ were taken with the Crystal Barrel detector at LEAR, using a $\bar{p}$ beam of 200 MeV/c stopping in liquid hydrogen. A full technical description of the detector has been given in Ref. [29]. The hydrogen target was surrounded by two cylindrical multiwire chambers for triggering, followed by a cylindrical jet drift chamber measuring charged particles. The outermost layers of this jet chamber covered $\sim 70\%$ of the solid angle. Surrounding this drift chamber was a barrel of 1380 CsI crystals detecting photons with good resolution and high efficiency over a solid angle 98% of 4π. A solenoidal magnet provided a field of 1.5T.

The present data sample consists of 9.4M triggered 4-prong events. The trigger selected long tracks having good momentum resolution in the drift chamber: it required hits in at least one of the two multiwire chambers and also in one of the first 3 layers of the drift chamber and at least one of the last 4. Off-line analysis selects ~ 2.5M events with four well reconstructed tracks conserving charge. Photons are selected by demanding a shower of at least 10 MeV in the CsI crystals. Energy deposits in the crystals matching up with charged tracks are eliminated. A small detail is that showers centred in crystals immediately adjoining the entrance or exit beam-pipe are rejected, because of the risk of shower energy being lost down the beam-pipe. These cuts reduce the sample from 2.5M to ~ 1.3M.

Events with 4 charged tracks and 2 or more γ are submitted to a 4C fit to $2\pi^+2\pi^-2\gamma$; 208K events survive with a confidence level $> 10\%$. Almost all come from events containing just 2 or 3 showers. In the latter case, one surplus shower is interpreted as arising from nuclear interactions of nearby charged particles in the CsI detectors, and this shower is discarded. Next, 5C kinematic fits are made to the two reactions

$$\bar{p}p \to 2\pi^+2\pi^-\eta, \ (\eta \to 2\gamma) \tag{1}$$
$$\to 2\pi^+2\pi^-\pi^0, \ (\pi^0 \to 2\gamma). \tag{2}$$

This gives 4020 events fitting the former hypothesis and 176,484 fitting the latter, both with confidence level $> 10\%$. Fig. 1 shows the η mass spectrum of events fitted to $\bar{p}p \to \pi^+\pi^-\pi^+\pi^-\gamma\gamma$ before kinematic fitting to reaction (1), and after rejecting events fitting reaction 2 with confidence level $> 0.1\%$. There is $< 5\%$ background under the η signal, which is centred at 548.3 MeV, close to the PDG value.

A Monte Carlo simulation of the detector and acceptance cuts using GEANT gives reconstruction efficiencies of 6.4% and 6.8% respectively for reactions (1) and (2). Using the known branching ratio for reaction (2) of $(17.3 \pm 1.5)\%$ [30], the branching fraction for reaction (1) is $0.90 \pm 0.15\%$ after correcting for all decay modes of the η, i.e. for the 39.25% branching ratio of $\eta \to \gamma\gamma$. Studies have also been made of (A) $\bar{p}p \to 2(\pi^+\pi^-)\eta$, $\eta \to 3\pi^0$ and (B) $\bar{p}p \to \pi^+\pi^-2\pi^0\eta$, $\eta \to \pi^+\pi^-\pi^0$. They will not be reported in detail, since they suffer from backgrounds under the η signals of $\sim 25\%$. Nonetheless, they may be used to check the branching fraction. From 6040 events of reaction (A), a branching fraction of $(0.97 \pm 0.09)\%$ is found. From 750 events of reaction (B), the branching ratio is $(1.00 \pm 0.12)\%$. Combining these values, the mean branching fraction is $(0.97 \pm 0.07)\%$.

3 The amplitude analysis

The minimal set of ingredients required by the amplitude analysis is:

$$\begin{aligned}
{}^1S_0 &\to \eta(1440)\sigma;\ \eta(1440) \to \eta\sigma \text{ and } a_0(980)\pi && (3)\\
&\to \eta(2190)\sigma;\ \eta(2190) \to \eta\sigma \text{ and } a_0(980)\pi && (4)\\
&\to f_0(1370)\eta;\ f_0(1370) \to \sigma\sigma \text{ and } \rho\rho && (5)\\
&\to \eta'(958)\sigma,\ \eta'(958) \to \eta\pi^+\pi^- && (6)\\
{}^3S_1 &\to [\eta'(958)\rho]. && (7)
\end{aligned}$$

A further channel for which there is some evidence is

$$^1S_0 \to \eta(1295)\sigma;\ \eta(1295) \to \eta\sigma \text{ and } a_0(980)\pi. \qquad (8)$$

Here σ means the $\pi\pi$ S-wave amplitude, for which we use the parametrisation of Zou and Bugg [31]. We adopt the Flatté form for the $a_0(980)$, with parameters from Ref. [32]. The $\eta(2190)$ is a shorthand for the broad $\eta\pi\pi$ signal which is observed lying beneath the narrow $\eta(1440)$ in $J/\Psi \to \gamma(\eta\pi\pi)$ [33]. There it makes an unmistakable broad physics background, and it is logical to include it here. It makes a significant contribution, but the analysis is not sensitive to this component being resonant or not. Effectively, it parametrises a broad coherent 0^- background in $\eta\pi^+\pi^-$. Ref. [33], Fig. 2(a), shows that it peaks in $\eta\pi\pi$ at ~ 1550 MeV with a width of ~ 400 MeV; this shape is created by competition between the $\eta\pi\pi$ channel and the opening of strong channels $\rho\rho$, $\omega\omega$ and K^*K^*. The full parametrisation of Ref. [33] is used here.

The overall approach in fitting the data is as follows. Firstly a fit is made using simple Breit-Wigner amplitudes of constant width for $\eta(1440)$ and $f_0(1370)$, optimising their masses and widths. At the second step, these forms are replaced by amplitudes with s-dependent widths which parametrise the s-dependence of the phase space for each decay channel; they use best estimates of branching ratios to fix the magnitude of each channel width. Thirdly, possible extra channels are considered and eliminated, as discussed in subsection 3.6. At the fourth and final step, the effect of triangle diagrams are considered for the decays of the $\eta(1440)$, $\eta(1295)$ and $\eta(2190)$. Except where stated otherwise, results are taken from this final step.

The Monte Carlo simulation of the cuts and the acceptance of the detector produces 20,630 events fitting to $\eta\pi^+\pi^-\pi^+\pi^-$; these are used in the maximum likelihood fit. An incoherent phase space background of 3% is included in the fit, so as to simulate background under the η peak of Fig. 1, but it has little effect.

3.1 Comparison with data

Figs. 2(a)–(f) show projections of data on to s, the square of the invariant mass M, for $\eta\pi$, $\eta\pi^+\pi^-$, $\pi^+\pi^-$, 4π, 3π and $\eta 3\pi$ combinations. Histograms show the fit; phase space is shown by the dashed curves. Slight fluctuations in both the fit and phase space arise from the limitation in Monte Carlo statistics.

In Fig. 2(a) the $a_0(980)$ is visible. The fit in the vicinity of the $a_0(980)$ is poor unless triangle graphs are included, as discussed in detail in Section 5. The fit shown in Fig. 2(a) includes these diagrams. At the lowest $\eta\pi$ masses, the fit is not quite perfect. This problem originates mostly from decays of the $\eta'(958)$, which makes particularly large contributions there. The $\eta'(958)$ has been fitted with a Gaussian width having a cross section with standard deviation $\sigma = 10.6$ MeV; its decays are approximated by $\eta\sigma$ phase space. The small discrepancy in Fig. 2(a) appears to be due to this approximation. If the η' is removed by a cut, the fit to the $\eta\pi$ mass distribution at low masses is good. However, it is not possible to fit the data with this cut, since reflections ('wrong combinations' using pions from the η') appear across the whole mass range of $\eta(1440)$. Fits with alternative treatment of the $\eta'(958)$ produce almost no changes in conclusions elsewhere.

The 2π mass spectrum, Fig. 2(c), is enhanced towards masses higher than phase space. This is because of the S-wave $\pi\pi$ interaction, σ. A single coupling constant is used for the σ over the whole mass range. In principle, this coupling constant may vary with s. It is possible to make a minor improvement in the fit to the 2π mass distribution by introducing such a form factor, but the improvement is small and has no effect elsewhere.

The 4π mass distribution of Fig. 2(d) is a major feature of the data. It peaks strongly at the highest masses compared with phase space, and suggests the presence of $f_0(1370)$. This is confirmed by the amplitude analysis. Fig. 3 shows the mass projection with $f_0(1370)$ omitted from the fit.

The 3π mass distribution of Fig. 2(e) again peaks at masses higher than phase space, but is otherwise featureless. Its shape is well fitted by reflections of other physics. The $\pi'(1300)$ is at too high a mass to have a significant effect. The $\eta 3\pi$ mass spectrum, Fig. 2(f), is close to phase space, but with a slight inflection near the mass of $a_0(1450)$ and a slight peak around 1580 MeV. However, both of these features may be fitted as reflections of other physics.

Fig. 2(b) shows a distinct shoulder in the region of $\eta(1440)$. It is possible to display the presence of this resonance more distinctly. One $\pi^+\pi^-$ combination, coming from the $\eta(1440)$ decay, always has quite a high mass. The resonance is accompanied by a spectator $\pi^-\pi^+$ combination from the production process; the mass of this spectator is necessarily restricted below $\sim$ 480 MeV. The $\eta(1440)$ may therefore be isolated by demanding one high mass $\pi^+\pi^-$ pair and one of low mass. Suppose we label particles $\pi_1^+\pi_2^+\pi_3^-\pi_4^-$. The quantity $R_{13} = (P_1 + P_3)/(P_2 + P_4)$ is formed and the alternative combination R_{14}; here $P = \sqrt{P_x^2 + P_y^2 + P_z^2}$. A simulation shows that over 90% of $\eta(1440)\sigma$ events have one value of R outside the range 0.6 to 1/0.6. In order to remove reflections from $\eta'(958)$, events having a combination with $M(\eta\pi^+\pi^-)$ within ± 30 MeV of the $\eta'(958)$ are rejected.

Fig. 4 shows events passing these cuts. The upper peak is centred at 1397 MeV, with a full width at half maximum of 50 MeV. The dashed curve shows phase space after the cut on R, and normalised to the mean of data and fit around $s = 1.5$ GeV^2. The cut on R produces a bias against the central mass region, but the $\eta(1440)$ signal produces an obvious peak well above this remaining phase space. The peak of events above phase space for low s is due to reflections from the $\eta(1440)$, i.e. wrong combinations. Fig. 4 is presented simply as visual evidence for $\eta(1440)$; all events, whether passing this cut or not, are used in the amplitude analysis.

Fig. 5(a) shows the $\eta\pi\pi$ mass projection calculated from the fit for one charge combination of $\eta(1295)$, $\eta(1440)$ and $\eta(2190)$. This is what one would see if the combinatorics could be eliminated. The broad $\eta(2190)$ produces a significant background under the $\eta(1440)$, as for $J/\Psi \to \gamma(\eta\pi\pi)$. Fig. 5(b) shows the projection on to $s(\eta\pi)$ from one charge combination of the fitted $\eta(1440)$. There is a deep dip at $s \simeq 0.95$ GeV^2 due to destructive interference between decays to $\eta\sigma$ and $a_0(980)\pi$. The dashed curve shows the contribution from decays only to $\eta\sigma$.

Initially $\eta(1440)$ is fitted with a Breit-Wigner resonance of constant width. Figs. 6(a) and (b) then show the variation of log likelihood with the mass and width of $\eta(1440)$. In making these scans, all coupling constants are re-optimised at each step. The mass of $\eta(1440)$ optimises at 1399 MeV with a statistical error of ± 4 MeV and with a width of 46 ± 6 MeV. (Our definition of log likelihood is such that a change of 0.5 corresponds to one standard deviation). However, interferences with the broad $\eta(2190)$ underneath $\eta(1440)$ are capable of shifting the mass by ± 15 MeV [4], which therefore represents a dominating systematic error. Coherent interference with this broad background has often been neglected in earlier work.

For final fits, the Breit-Wigner amplitude of the $\eta(1440)$ is replaced by the s-dependent form of the BES group [34]; there is a minor improvement in log likelihood of 12.4.

The Obelix group [35] has claimed a second narrow $\eta(1465)$ decaying to $[K^*(890)K]$ with $\ell = 1$. We have searched for its possible $\eta\pi^+\pi^-$ decay, by inserting into the analysis a resonance with their width and scanning its mass. We find no evidence for its presence.

3.2 $\eta(1295)$

When $\eta(1295)$ is inserted into the fit, there is a weak optimum for its mass at 1255 ± 10 MeV and for its width at 90 ± 23 MeV. It improves log likelihood by 23 with these parameters. However, in Fig. 5(a), which shows the mass projection from one combination of $\eta(1295)$, $\eta(1440)$ and $\eta(2190)$, there is no peak at 1255 or 1295 MeV, but simply an interference effect. Also we find dominant decays to $\eta\sigma$, whereas earlier data have preferred $a_0(980)\pi$ decays [5]. Therefore we are not confident of the presence of $\eta(1295)$ and will regard the fitted signal as an upper limit. In the final fit, the mass and width of $\eta(1295)$ are fixed at PDG values.

In order to display the significance of each element in the fit, Table 2 summarises the change in log likelihood when each signal is omitted and remaining contributions are re-optimised. Our experience elsewhere is that a change of 40 is highly significant. For $\eta(1295)$, the change in log likelihood is larger when both decay modes are omitted than when either one or the other is dropped, but is still < 40; the fit can move cross section between these two decay modes. A large ambiguity also exists between $^1S_0 \to \eta'\sigma$ and $^3S_1 \to \eta'\rho$. The convergence of the fit is rapid and secure (25–30 iterations from a random starting point) and requires less than one minute of computing. Consequently, we have been able to experiment with a large variety of assumptions in order to assess systematics.

Channel	ΔS	BR $\times 10^4$
$\eta(1295) \to \eta\sigma$	12	2.8
$\eta(1295) \to a_0(980)\pi$	0.5	0.1
$\eta(1295)$ interference $\eta\sigma \times a_0(980)\pi$	-	-0.1
All $\eta(1295)$	23	2.8
$\eta(1440) \to \eta\sigma$	70	23.1
$\eta(1440) \to a_0(980)\pi$	140	9.6
$\eta(1440)$ interference $\eta\sigma \times a_0(980)\pi$	-	-21.8
All $\eta(1440)$	158	10.9
${}^1S_0 \to \eta(2190)\sigma;\ \eta(2190) \to \eta\sigma$	69	28.1
${}^1S_0 \to \eta(2190) \to a_0(980)\pi$	29	8.3
$\eta(2190)$ interference $\eta\sigma \times a_0(980)\pi$	-	-22.6
All $\eta(2190)$	82.5	13.8
$f_0(1370) \to \sigma\sigma$	426	30.7
$f_0(1370) \to \rho\rho$	384	19.1
$f_0(1370)$ interference $\sigma\sigma \times \rho\rho$	-	-0.1
All $f_0(1370)$	539	49.7
${}^1S_0 \to \eta'\sigma$	144	16.5
${}^3S_1 \to \eta'\rho$	14	5.6
Both $\eta'(958)$	1027	22.1

Table 2

Changes in S = log likelihood when channels are removed from the reference fit and remaining contributions are re-optimised. The final column gives branching fractions (BR) (in units of 10^{-4}) for $\bar{p}p$ annihilations to channels with the charges of present data, from squares of amplitudes, see text.

3.3 A possible relation between $\eta(1440)$ and $\eta(2190)$

The relative branching ratio of $\eta(1440)$ to $a_0(980)\pi$ and $\eta\sigma$ in Table 2 is the same within errors as for $\eta(2190)$. Furthermore, the relative phases of these processes are also the same within an error of $\pm 15°$. One can fit the same ratio and phase to both with a penalty in log likelihood of only 3.4, which cannot be considered significant for two parameters.

This relation between $\eta(1440)$ and $\eta(2190)$ may not be accidental. Quantum mechanical mixing between $\eta(2190)$ and $\eta(1440)$ will inevitably occur. Suppose the same component of the wave function (e.g.a glueball component) is responsible for decays to $\eta\sigma$ and $a_0(980)\pi$ in both $\eta(1440)$ and $\eta(2190)$. This could explain the observations.

3.4 Branching fractions

The last column of Table 2 shows branching fractions of individual channels. Evaluation of these branching fractions is confused by large interferences. If one reconstructs the $\eta(1440)$ contribution to one combination of charges, as in Fig. 5(a), the $\eta(1440)$ appears as a peak above a slowly varying background. The peak gives a branching ratio of 1.5×10^{-3} of all $\bar{p}p$ interactions. However, we shall now show that interferences, particularly between $\eta(1440)$ and the broad $\eta(2190)$, can alter this estimate by a factor 1.4.

The procedure used here for evaluating branching fractions is described in an earlier paper on $\bar{p}p \rightarrow 5\pi^0$ at rest [24], where similar large interferences arise. Our objective is to determine the branching fractions of individual resonances, omitting interferences with the spectator or with other channels. Such interferences are due to the environment of $\bar{p}p$ annihilation and need to be decoupled from the properties of a resonance as it would appear 'in free space', i.e. as an isolated resonance. We first fit the data including all interferences and normalise to the 0.97% branching fraction of $\bar{p}p \rightarrow \eta\pi^+\pi^-\pi^+\pi^-$. This determines coupling constants absolutely. Branching fractions are then evaluated from the modulus squared of each amplitude, allowing for the charge combinations in present data, and integrating over the available phase space. Interferences between channels and between charge combinations are eliminated in this procedure. Nonetheless, interference within one charge combination is evaluated, e.g. between $\eta(1440) \rightarrow \eta\sigma$ and $\eta(1440) \rightarrow a_0\pi$, since it is a property of the resonance however it may be produced. Table 2 shows branching fractions calculated in this way. Interference terms contribute negative amounts if the interference is destructive. The destructive interference between the two decay modes of $\eta(1440)$ has a large effect, as does interference with $\eta(2190)$. The total branching fraction for $\eta(1440)$ drops by a factor 1.4.

3.5 $f_0(1370)$

Table 2 shows that the $f_0(1370)$ makes a very large improvement in log likelihood of 539. The full multi-dimensional dependence of the amplitudes separates $\sigma\sigma$ and $\rho\rho$ decays via their quite different angular dependence (isotropic for $\sigma\sigma$, but dependent on the dot product $q_1.q_2$ between momenta q_i of pions from the decay of each ρ). The $f_0(1370)$ is well separated from the other broad contribution from $\eta(2190)$, because the latter peaks towards an $\eta\pi\pi$ mass of 1550 MeV.

The branching fractions given in Table 2 correspond only to charges observed in present data. A point of interest is the relative branching ratio of $f_0(1370)$ to $\sigma\sigma$ and $\rho\rho$. It is necessary to correct for other charge states $\pi^+\pi^-\pi^+\pi^-$ and $4\pi^0$ in the decays of $\sigma\sigma$ and $\rho\rho$. Interferences are important within each of these and may be different from present data. Chen, Li and Zou [36] have recently investigated these interferences and we draw on their conclusions. One might naively expect $\sigma\sigma$ to decay to $\pi^+\pi^-\pi^+\pi^-$, $\pi^+\pi^-\pi^0\pi^0$, and $4\pi^0$ in the ratio of charge combinations 4 : 4 : 1; Chen et al. show that, including interferences, the branching fraction for $\pi^+\pi^-\pi^+\pi^-$ needs scaling by a factor 1.91 instead of 2.25. For $\rho\rho$ one expects a factor 3; it turns out that interferences for this channel are the same for all charge states, so this result survives. The branching ratio between $\rho\rho$ and $\sigma\sigma$ for all decays is then

$$\frac{BR[f_0(1370) \to \rho\rho]}{BR[f_0(1370) \to \sigma\sigma]} = 0.98 \pm 0.25, \tag{9}$$

where the error is mostly systematic; it covers the range of fits which have been obtained with varying forms for $f_0(1370)$ and other components. The total branching fraction for $\bar{p}p \to f_0(1370)\eta$ for all charges is:

$$BR[\bar{p}p \to f_0(1370)\eta] = (1.16 \pm\ 0.16) \times 10^{-2}. \tag{10}$$

These values of course refer only to the phase space available in the present reaction, i.e. up to 1330 MeV. If the phase space were to extend over the whole resonance, the branching ratio of equn. (9) would be different. Phase space for $\rho\rho$ rises slightly faster than that for $\sigma\sigma$ because the ρ is narrower. On the other hand, the phase space for each σ increases with the available 4π mass. It is difficult to estimate the magnitude of these effects precisely unless the mass and width of $f_0(1370)$ are known accurately. With the parameters assigned below in Section 4, the two effects cancel, leaving equn. (9) approximately unchanged.

To estimate the branching ratio of $f_0(1370)$ between $\Gamma_{2\pi}$ and $\Gamma_{4\pi}$, we compare with data on $\bar{p}p \to \eta\pi^0\pi^0$ at rest. Fig. 7 reproduces the amplitude fitted to the latter data in Ref. [22], Fig. 3(c). The presence of $f_0(1370)$ is suggested by the loop which begins to form at the highest masses near 1.3 GeV. The branching fraction of the whole channel for $\bar{p}p \to \eta\pi^0\pi^0$ is only 6.8×10^{-3}, which is smaller than the branching fraction in equn. (10). The contribution of $f_0(1370)$ to the $\eta\pi^0\pi^0$ data is clearly a small proportion of this, but it is debatable just how big this contribution is. Abele et al. [22] fitted the $\eta\pi^0\pi^0$ data using a Breit-Wigner amplitude of constant width for $f_0(1370)$. That assumption no longer appears adequate, with the consequence that their evaluation of the branching fraction for $\bar{p}p \to f_0(1370)\eta$, $f_0(1370) \to \pi^0\pi^0$ may be too low. This branching fraction is proportional to the square of the radius of the $f_0(1370)$ loop on Fig. 7, compared with the mean square amplitude. However, there is a large interfering contribution from the broad $f_0(400-1200)$. This large term and flexibility in its interferences with $f_0(1370)$ prevents a clear assessment of the $f_0(1370)$ component. From a re-analysis of the $\eta\pi^0\pi^0$ data, we estimate that it could contribute anywhere from 2 to 10% in intensity. Allowing for $\eta\pi^+\pi^-$ contributions, this branching fraction is multiplied by a factor 3 with the result $BR[\bar{p}p \to f_0(1370)\eta,\ f_0(1370) \to 2\pi] = (0.4 - 2.0) \times 10^{-3}$. Using equn. (10), the resulting value of $\Gamma_{2\pi}/\Gamma_{4\pi}$ is in the range 3–18%. The best prospect for determining $\Gamma_{2\pi}/\Gamma_{4\pi}$ appears to be via a combined analysis of data on $\bar{p}p \to 3\pi^0$ and $\bar{p}p \to 5\pi$ at rest, or from a corresponding analysis of central production data. Those data have the big advantage of covering the whole mass region of $f_0(1370)$.

From present data, the essential point is that decays to 4π are much stronger than to 2π, by at least a factor 5. This ratio is far too large for the signal to be attributed to $f_2(1270)$ or $f_0(1500)$ or the broad component of the $\pi\pi$ S-wave. We now amplify this discussion.

Firstly, the branching fraction for production of $f_2(1270)$ in $\eta\pi^0\pi^0$ data is very small: $(2 \pm 0.8) \times 10^{-6}$ [22], because of the $L = 2$ centrifugal barrier for its production. The predicted rate for production of $f_2(1270)$ in $\eta\pi^+\pi^-\pi^+\pi^-$ is then a factor 10^4 smaller than derived in equn. (10) for $f_0(1370)$. This is completely negligible.

Secondly, there is a well known very broad component in the $\pi\pi$ S-wave in the 400–1500 MeV mass range, called $f_0(400-1200)$ by the PDG. The analysis of CERN-Munich data [9,12] shows that this component is almost elastic up to 1330 MeV: $\Gamma(2\pi)/\Gamma(4\pi) > 5$, in strong contradiction with the branching ratio deduced here for $f_0(1370)$. It could only account for at most 5% of the 4π signal observed here.

Thirdly, let us consider $f_0(1500)$. Data from the Crystal Barrel Collaboration in several 5π channels have been presented at Hadron'97 [13]. These data show that the branching ratio for $f_0(1500) \to 4\pi$ is about a factor 2 stronger than to 2π, in reasonable agreement with analysis of CERN-Munich data [12]; our recent unpublished update of this analysis finds a factor 1.5 ± 0.5.

Furthermore the ratio $4\pi/2\pi$ rises with 4π mass. There is no possibility that $f_0(1500)$ accounts for present data. Because of the narrow width of $f_0(1500)$, namely 120 ± 19 MeV [5], it could account only for a small component of the 4π signal observed here. Experimentally, a fit using that hypothesis gives log likelihood worse by 32.3 than that presented here. Our conclusion is that we are observing the dominant decays of $f_0(1370)$ to 4π.

This is an important result. Minkowski and Ochs [37] have argued against the existence of $f_0(1370)$ because it is not visible in CERN-Munich data. However, the magnitude of signal it produces in $\pi\pi \to \pi\pi$ is proportional to $(\Gamma_{2\pi}/\Gamma_{tot})^2$; if $\Gamma_{4\pi}/\Gamma_{2\pi} > 5$, its contribution to CERN-Munich data is too small to be visible. In $\bar{p}p \to 3\pi^0$ and $\bar{p}p \to \eta\pi^0\pi^0$, its magnitude is instead proportional to $g^2\Gamma_{2\pi}/\Gamma_{total}$, where g is the coupling constant for $\bar{p}p \to f_0(1370)\eta$; the linear dependence on $\Gamma_{2\pi}/\Gamma_{total}$ explains why it is visible in $\bar{p}p$ annihilation at rest.

A question presently under debate is why a peak appears in $\pi\pi \to KK$ at ~ 1300 MeV. Its magnitude there is proportional to $\Gamma_{2\pi}\Gamma_{KK}/\Gamma^2_{tot}$. Minkowski and Ochs argue that this peak can be fitted with destructive interference involving $f_0(1500)$, but without any contribution from $f_0(1370)$. To explain the observed peak in terms of $f_0(1370)$ would require that $\Gamma_{2\pi}$ and Γ_{KK} should both be close to 20% of Γ_{tot} at 1300 MeV; these values are towards the top of the allowed range. The ratio $\Gamma_{2\pi}\Gamma_{KK}/\Gamma^2_{total}$ will be strongly s-dependent and largest at low masses. Hence a fresh fit to these data and $\bar{p}p \to 3\pi^0$ is required using the s-dependent width for $f_0(1370)$ discussed in the next section; this will be the subject of a separate paper.

3.6 Ingredients not required by the fit

We have tried adding $a_0(1450)\pi$, $a_0(1450) \to a_0(980)\sigma$ to the analysis. Log likelihood improves by 32. However, there is no optimum when the mass and width of $a_0(1450)$ are scanned, so there is no clear evidence for its presence. The problem is that the $a_0(1450)\pi$ channel is easily confused with channel (4): $\eta(2190)\sigma$, $\eta(2190) \to a_0(980)\pi$. In $\eta\pi^0\pi^0$ data, the $a_0(1450)$ signal is small, though distinct: it contributes only 3% to those data [22]. In the present data, the $a_0(1450) \to a_0(980)\sigma$ signal could be as large as 12%. The result is only a poor limit on the branching ratio $BR[a_0(1450) \to a_0(980)\sigma]/BR[a_0(1450) \to \eta\pi] \leq 4.3$.

Adding $\hat{\rho}(1405)$ to the fit with $M = 1400$ MeV, $\Gamma = 310$ MeV from recent Crystal Barrel work [38] gives negligible improvement in log likelihood. It is nonetheless useful to establish upper limits on its contribution. We have determined the magnitudes of contributions from those channels which make log likelihood worse by 4.5, i.e. statistically a 3σ effect. Results are given in

Table 3.

Channel	Fraction of present data (%)
${}^1S_0 \to \hat{\rho}(1405)\pi,\ \hat{\rho} \to f_1(1285)\pi$	0.65
${}^1S_0 \to \hat{\rho}(1405)\pi,\ \hat{\rho} \to b_1(1235)\pi$	0.88
${}^3S_1 \to \hat{\rho}(1405)\pi,\ \hat{\rho} \to f_1(1285)\pi$	0.45
${}^3S_1 \to \hat{\rho}(1405)\pi,\ \hat{\rho} \to b_1(1235)\pi$	2.32

Table 3
Contributions to present data from $\hat{\rho}$ making log likelihood worse by 3 standard deviations.

Other channels which have been tried (improving log likelihood in every case by < 10) are

$$
\begin{aligned}
{}^1S_0 &\to [f_1(1285)\sigma]_{\ell=1} \\
&\to [f_1(1420)\sigma]_{\ell=1};\ f_1(1420) \to a_0(980)\pi \ \mathit{or}\ \eta\sigma \\
&\to [b_1(1235)\rho]_{\ell=0};\ b_1(1235) \to \eta\rho \\
{}^3S_1 &\to [\rho'(1465)\sigma]_{\ell=0};\ \rho'(1465) \to [\eta\rho]_{\ell=1} \\
&\to [\rho'(1465)\eta]_{\ell=1};\ \rho'(1465) \to [\rho\sigma]_{\ell=0} \\
&\to [f_1(1285)\rho]_{\ell=0} \\
&\to [b_1(1235)\sigma]_{\ell=1};\ b_1(1235) \to \eta\rho \\
{}^3P_1 &\to [f_1(1285)\sigma]_{\ell=0}.
\end{aligned}
$$

Here ℓ is the orbital angular momentum in the production process. These reactions are unlikely, because of centrifugal barriers or high thresholds or because they require P-state annihilation. Centrifugal barriers are standard Blatt-Weisskopf forms with a radius of interaction of 0.8 fm. There is tentative evidence for a very small $f_1(1285)$ signal, but it is at most a 2.5σ effect.

4 Parametrisation of $f_0(1370)$

Initial fits to data were made using a Breit-Wigner amplitude for $f_0(1370)$ of constant width. The mass optimises at ~ 1290 MeV; the width optimises at 300 MeV, but fits of similar quality are obtained with widths over the range 235 to 380 MeV. The fitted mass is close to the top of the available 4π phase space, so one cannot expect these fitted values to be accurate. We shall now explore in some detail the effect of this s-dependence.

The phase space for the 4π channel is strongly s-dependent and it is logically necessary for consistency to include this s-dependence into the Breit-Wigner denominator. This is the requirement of unitarity. We have calculated the s-dependence of the Lorentz invariant phase space $\rho(s)$ for $\sigma\sigma$ and $\rho\rho$ using equn. (40) of Ref. [12]:

$$\rho_{4\pi}(s) = \int_{4m_\pi^2}^{(\sqrt{s}-2m_\pi)^2} \frac{ds_1}{\pi} \int_{4m_\pi^2}^{(\sqrt{s}-\sqrt{s_1})^2} \frac{ds_2}{\pi} \frac{8|q|\ |q_1|\ |q_2|}{\sqrt{s\ s_1\ s_2}} |T_1(s_1)|^2 |T_2(s_2)|^2 \exp(-\alpha |q|^2). \quad (11)$$

Here q_1 and q_2 are momenta of pions from decay of each σ or ρ in its rest frame, and q is the momentum of the σ or ρ in the rest frame of $f_0(1370)$; T_1 and T_2 are amplitudes for ρ or σ decays. Fig. 8 shows $\rho(s)$ for a variety of form factors $\exp(-\alpha q^2)$ for the production process, with α varying from zero to 6 GeV^{-2}. The exponential affects the phase space strongly only for masses far above that relevant to the present data, but it does affect the slope of the phase space as a function of $s = M^2$, even for low masses. The curves of Fig. 8 may be parametrised by the empirical form:

$$\rho(s) = \frac{A + Bs + Cs^2}{1 + \exp[D(E-s) + Fs^2 + Gs^3]}. \quad (12)$$

Table 4 gives values of the parameters, in the hope that these parametrisations may be useful in further work.

The Breit-Wigner form we take for $f_0(1370)$ is:

$$f = \frac{1}{s - M_0^2 - m(s) + iM_0[\Gamma_{2\pi} + \Gamma_{KK}(s) + \Gamma_{\eta\eta}(s) + \Gamma_{\rho\rho}(s) + \Gamma_{\sigma\sigma}(s)]}. \quad (13)$$

We take $\Gamma_{2\pi}$ to be constant (since the threshold is distant), but take all other Γ to be proportional to the available phase space $\rho(s)$ for decay, including the exponential form factor. The corresponding K-matrix elements are $K_{ij} = g_i g_j/(s - M_0^2)$, (where g are coupling constants), so M_0 is the mass of the K-matrix pole.

The quantity $m(s)$ in the denominator of equn. (13) is a dispersive correction to the mass:

$$m(s) = \frac{(s - M_0^2)}{\pi} \int ds' \frac{M_0 \Gamma_{total}(s')}{(s' - M_0^2)(s' - s)}. \quad (14)$$

This term is necessary to make equn. (13) fully analytic. We find that it plays a major role.

The contributions to $\Gamma(s)$ need input from other sources. We adopt coupling constants fitted to a large data-base by Anisovich et al. [39]. For this solution, coupling constants are such that, at the $f_0(1370)$ third-sheet pole, $\Gamma_{2\pi} : \Gamma_{KK} : \Gamma_{\eta\eta} : \Gamma_{4\pi} = 1 : 0.24 : 0.13 : 4.96$; the value of $\Gamma_{2\pi}$ is close to the maximum value

Channel	α	A	B	C	D	E	F	G
$\sigma\sigma$	0	0.7535	-3.1275	3.1369	2.7698	1.6304	0.2798	-
	1	0.4981	-2.1283	2.2211	3.6277	1.4193	0.4251	-
	2	0.3547	-1.6050	1.7969	4.5431	1.2896	0.6618	-
	3	0.0791	-0.7415	1.3007	5.3429	1.2657	0.8117	-
	4	-0.2134	0.1223	0.8760	5.7038	1.2879	0.8638	-
	5	-0.3846	0.6540	0.5853	5.8868	1.3001	0.8786	-
	6	-0.4498	0.8857	0.4064	5.9783	1.2957	0.9027	-
$\rho\rho$	0	-3.2278	7.7632	0.1665	9.9221	1.1883	3.1276	-0.5343
	1	-4.3023	10.6713	-1.1290	9.0618	1.1981	3.1859	-0.5477
	2	-4.3479	11.1398	-1.6542	9.9198	1.1411	3.7098	-0.6547
	3	-3.9086	10.5712	-1.8097	11.3529	1.0632	4.5717	-0.8255
	4	-2.5078	9.1625	-1.7253	13.5015	0.9881	5.7774	-1.0523
	5	5.9635	3.6617	-0.9976	16.0788	0.9717	6.8497	-1.2092
	6	11.3862	-1.2680	-0.3091	16.4636	0.9916	6.8823	-1.1986

Table 4
Parameters in equn. (12) with s in GeV^2.

consistent with no structure in Cern-Munich data around 1300–1370 MeV [12]. Magnitudes of widths in equn. (13) are adjusted to reproduce these values. The fit to the present data is actually quite insensitive to the coupling to $\pi\pi$, $\eta\eta$ and KK, but the following discussion comments on the fits to $f_0(1370)$ in other data.

The line shape predicted for the 2π and 4π channels is illustrated in Fig. 9 for the parameters given below for our final fit. The 2π and 4π cross sections are shown by full and dashed lines, normalised to 1 at each peak. Both peaks are somewhat asymmetric. The 2π channel is cut off strongly at high masses by the rapidly increasing 4π width; the fall above the peak is faster than the rise to the peak. The converse applies to the 4π channel, because of the increasing 4π phase space. As a measure of the position and width of each peak, we determine the mass at half-height on each side of the peak; the average mass $\bar{M}$ is then taken as the mean of these values and the mean width $\bar{\Gamma}$ as the difference. These are approximately the values which will be obtained in fits with a Breit-Wigner amplitude of constant width. Fig. 9 and Table 5 below show that the 4π peak is centred 50–100 MeV above the 2π peak, because of the rapidly rising phase space for 4π.

The dash-dotted curve on Fig. 9 shows the line-shape of $f_0(1370)$ as it will appear in $\bar{p}p \to \eta(4\pi)$, modified by the available phase space; in this calculation, the cross section $|f|^2$ from equn. (13) is multiplied by $k/\sqrt{s}$, where k is the momentum with which $f_0(1370)$ is produced in $\bar{p}p \to f_0\eta$.

A somewhat surprising result is that it is not possible to find a reasonable set of parameters giving a full-width $\bar{\Gamma}_{4\pi}$ greater than ~ 260 MeV; a smaller value appears more likely. Table 5 gives values of $\bar{M}$ and $\bar{\Gamma}$ for a variety of values of $\Gamma_{2\pi}$ and the parameter α appearing in the form factor. All are evaluated for a value of $M_0 = 1400$ MeV for the resonance mass. The narrow width is analogous to that observed for $a_0(980)$ and $f_0(980)$ and arises from damping of the resonance by the strong 4π channel, i.e. by the effect of unitarity.

The first surprise is that $\bar{\Gamma}$ for both 2π and 4π channels vary only slowly with the magnitude of $\Gamma_{2\pi}$. The second surprise is that the magnitude of α, the form factor coefficient, has a comparable effect. We now outline how these results arise.

α (GeV)$^{-2}$	$\Gamma_{2\pi}$ (MeV)	$\bar{M}_{2\pi}$ (MeV)	$\bar{\Gamma}_{2\pi}$ (MeV)	$\bar{M}_{4\pi}$ (MeV)	$\bar{\Gamma}_{4\pi}$ (MeV)
1	30	1349	159	1396	172
	60	1333	177	1391	188
	120	1322	189	1387	199
3	30	1332	182	1393	202
	60	1308	205	1383	220
	120	1290	222	1375	232
6	30	1318	200	1390	232
	60	1283	226	1374	251
	120	1259	242	1359	260

Table 5
Values of $\bar{M}$ and $\bar{\Gamma}$ for a variety of values of α and $\Gamma_{2\pi}$.

The dispersive correction $m(s)$ is evaluated with a subtraction on resonance. Any constant contribution to $\Gamma(s)$ then makes no contribution to $m(s)$. For our final fit, $m(s)$ is shown in Fig. 10. It makes a large contribution to the Breit-Wigner denominator and its magnitude is controlled almost completely by $\Gamma_{4\pi}$, which varies most rapidly with s. The approximately linear variation with s of both $m(s)$ and $\Gamma_{4\pi}$ near 1370 MeV overwhelms the effect of the term $(s - M^2)$ in the Breit-Wigner denominator. In considering the mass range around 1300–1400 MeV, it is therefore helpful to rewrite equn. (13) as:

$$f \propto \frac{1/\Gamma_{total}(s)}{(s - M_0^2)/\Gamma_{total} - m(s)/\Gamma_{total} - iM_0}. \tag{15}$$

The effect of varying the strength of the coupling constants appears in the denominator only in the first term; when Γ_{total} is large, variations in it renormalise the overall strength of the Breit-Wigner amplitude via the numerator, but have only a small effect on its shape. The width of each peak is instead sensitive to the slope of $\Gamma_{4\pi}$ against s via $m(s)$. Hence it is sensitive to the form factor and α; larger widths are obtained with slower variation of $\Gamma_{4\pi}$, hence a stronger form factor.

Several determinations in Table 1 of the resonance mass from 4π data favour values around 1390 MeV, while our own determination from 2π data [22] is 1315 MeV with a width of ~ 230 MeV. This difference in mass is in accord with the differences displayed in Table 5. The pole position of the T-matrix is given by the mass at which the magnitude of the Breit-Wigner amplitude varies fastest. Since $\Gamma_{2\pi}$ is taken to be constant, the pole position is given by the fit to the 2π cross section, i.e. close to $1315 - i115$ MeV.

Fits to present data are insensitive to $\Gamma_{2\pi}$ and α. To select a set of values, we argue as follows. A typical width for high mass resonances listed by the PDG is 250 MeV, so if the 2π width is 20% of this, as in Ref. [39], a reasonable expectation is a value $\Gamma_{2\pi} \simeq 50$ MeV. Secondly, the form factor $\exp(-\alpha q^2)$ corresponds to a Gaussian source of radius R. With R in fm, $\alpha = (R/0.19732)^2/6$ GeV^{-2}. A radius of 0.5–0.8 fm corresponds to $\alpha = 1.1$ to 2.7 GeV^{-2}. We choose $M_0 = 1400$ MeV, $\Gamma_{2\pi} = 60$ MeV, and $\alpha = 3$ GeV^{-2} to obtain $\bar{M}_{2\pi} = 1308$ MeV, $\bar{\Gamma}_{2\pi} = 205$ MeV, close to our values obtained from 2π data. The fit to present data is quite insensitive to variations of parameters over the range shown in Table 5. However, it is not possible to obtain a width as large as some values ≥ 300 MeV in Table 1 without unreasonably large values of $\Gamma_{2\pi}$ or α. This suggests that some widths in Table 2 are a little high, possibly because of problems in separating $f_0(1370)$ and $f_0(1500)$, or possibly due to the overlap of these resonances.

5 $\eta(1440)$ and triangle graphs

The Dalitz plot for the $\eta(1440)$ may be made visible using cuts for the R parameter described in Section 3.1. This Dalitz plot is shown in Fig. 11(a). It contains some background contribution surviving the cut; this is included explicitly in the fits presented here. The $\eta\pi$ mass projection shown on Fig. 11(d) has a dip at $M_{\eta\pi} \simeq 0.95$ GeV, due to destructive interference between

$a_0(980)$ and the $\eta\sigma$ term, whose projection on to $\eta\pi$ mass produces a broad structureless cross section, shown by the dashed histogram on Fig. 5(c).

The data rise to a strong $\eta\pi$ peak significantly (30–50 MeV) above the mass normally attributed to $a_0(980)$. This feature is also visible in earlier Crystal Barrel data on $\bar{p}p \to \eta\pi^+\pi^-\pi^0\pi^0$, [3], see Fig. 5 there. These distinctive features have a natural and simple explanation in terms of triangle diagrams involving rescattering of decay products of the $\eta(1440)$.

The diagrams we consider are shown in Fig. 12. The large ones are Figs. 12(b), (c) and either or both of (e) and (f); Fig. 12(d) makes only a small contribution. We use K_0 to denote the $K\pi$ S-wave amplitude, which is fitted to the LASS data [40]. The terms of most interest here are Figs. 12(e) and (f), where decays of $\eta(1440)$ through K_0K or K^*K lead to rescattering of KK through the $a_0(980)$ at masses above the KK threshold to $\eta\pi$. [There are a further 10 triangle diagrams leading to $KK\pi$ final states not considered here].

The relevant formulae are based on the dispersion relation technique [41]. The amplitude of Fig. 12(a) may be written as:

$$B(s_{13}) = \lambda_{\eta\sigma} A_{\sigma\to\pi\pi}(s_{13}), \tag{16}$$

where $\lambda_{\eta\sigma}$ is the coupling constant for direct production of the $\eta\sigma$ final state in decays of $\eta(1440)$. The amplitude for the triangle diagram of Fig. 12(b) is then

$$\Delta(s_{12}) = \lambda_{\eta\sigma} \int\limits_{(M_1+M_2)^2}^{\infty} \frac{ds'_{12}}{\pi} \frac{\rho_{12}}{(s'_{12}-s_{12})} A_{\pi\eta\to\pi\eta}(s'_{12}, s_{12}) \int\limits_{C(s'_{12})} \frac{dz_{13}}{2} A_{\sigma\to\pi\pi}(s'_{13}), \tag{17}$$

where ρ_{12} is the two-particle phase space factor

$$\rho_{12}(s'_{12}) = \frac{1}{16\pi s'_{12}} \sqrt{[s'_{12}-(M_1+M_2)^2]\,[s'_{12}-(M_1-M_2)^2]}, \tag{18}$$

$$s_{13} = (P_3+P'_1)^2 = M_1^2 + M_3^2 - 2P'_{10}P_{30} + 2z_{13} \mid \vec{P}'_1 \mid\mid \vec{P}_3 \mid, \tag{19}$$

$$P'_{10} = \frac{s'_{12}+M_1^2-M_2^2}{2\sqrt{s'_{12}}}, \qquad \mid \vec{P}'_1 \mid = \sqrt{(P'_{10})^2 - M_1^2}, \tag{20}$$

$$P_{30} = \frac{s'_{12}+M_3^2-s_{12}}{2\sqrt{s_{12}}}, \qquad \mid \vec{P}_3 \mid = \sqrt{P_{30}^2 - M_3^2}. \tag{21}$$

Here P are 4-momenta and a prime denotes a particle in the intermediate state; $z_{13} = \cos\theta_{13}$ and θ_{13} is the angle between particles 1 and 3 in the centre of mass of particles 1 and 2. The second integration is carried out along a contour $C(s'_{12})$ described in detail in ref. [41]. For small s'_{12}, it coincides with $1 \le z_{13} \le 1$; it contains an additional piece at large s'_{12}.

Amplitudes for diagrams of Figs. 12$(c)-(e)$ are obtained by straightforward rearrangements of vertices and kinematic variables. For Fig. 12(f), the P-wave dependence of the $\eta(1440) \to K^*K$ production vertex and the K^* decay must be included. Triangle diagrams for decays of $\eta(2190)$ and $\eta(1295)$ are introduced as for $\eta(1440)$.

Using dispersion theory allows us to work with physical amplitudes, so we need not introduce any additional form factors as in the Feynman diagram technique. The $\pi\pi$ S-wave amplitude of Zou and Bugg [31] falls to a low value at a mass of ~ 1.5 GeV, and we use this as a natural cut-off for the dispersion integral over the σ amplitude. One subtraction is made in the dispersion integrals, and absorbed into the parameters λ, which are fitted to present data, but then checked against available information of branching ratios. The subtraction allows rapid converence of the dispersion integrals, so that the high energy behaviour does not influence the calculation significantly.

We now return to the essential features of the data. Firstly, the intensity observed in Fig. 11(a) is far from uniform along the $a_0(980)$ bands, the behaviour expected for a spin 0 resonance. Obviously there must be interferences or dynamics modifying the Dalitz plot. The intensity peaks strongly at an $\eta\pi$ mass just above 1 GeV, near the edge of the Dalitz plot. This peaking is not easily reproduced without triangle graphs. If triangle graphs are all omitted, log likelihood is worse than the best fit by 62.7. The problem with this type of fit is that, if the $a_0(980)$ amplitude is increased enough to approximate the peak of Fig. 11(d) at $s(\eta\pi)$ above 1 GeV^2, it produces a conspicuous cross (absent from the data) where the two $a_0(980)$ bands intersect. Also, the $\eta\sigma$ amplitude becomes so large as to produce an unacceptable band towards the lower left-hand edge of the Dalitz plot of Fig. 13(b). These problems are visible in a diluted form in Fig. 13, the best fit without triangle diagrams but still a poor fit.

In contrast, Fig. 11(d), which includes the triangle amplitudes, shows that they remedy this situation rather simply. Projections on to $\eta\pi$ and $\pi\pi$ mass are shown by histograms in Figs. 11(c) and (d) and compare quite well with the data.

The primary role is played by Figs. 12(d) and 12(e). There, a KK intermediate state de-excites via $a_0(980) \to \eta\pi$. In the language of nuclear physics, this is a two-step process. The rapidly expanding KK phase space factor $\rho(s'_{12})$ more than compensates for the rapid fall of the $a_0(980)$ amplitude above the KK threshold, and reproduces the strong peak in Fig. 11(d). Intermediate K_0K states of Fig. 12(e) have effects rather similar to K^*K of Fig. 12(f), so separating these two contributions is not crucial in fitting the present data. The reason is that both K_0K and K^*K amplitudes cover large regions of KK mass, and lead to differences only of fine detail in the $\eta\pi$ mass spectrum;

the K_0K intermediate state gives a slightly broader $a_0(980)$ peak than K^*K. However, resolving possible contributions to the $KK\pi$ channel will require a detailed fit to $KK\pi$ data simultaneously with $\eta\pi\pi$, including the complete set of 15 triangle graphs. Presently the $KK\pi$ data are not available to us.

Other triangle graphs such as Figs. 12(b) and (c) make sizable contributions. However, they vary slowly across the full Dalitz plot, and are readily interchanged in the fit with other broad contributions. Fig. 14 shows the fit keeping only the triangle graphs of Figs. 12(d) and (e). This fit is hardly distinguishable from that of Fig. 11, with all triangle graphs. Its log likelihood is worse than Fig. 11 only by 7.7.

It needs to be emphasised that the triangle diagrams are unavoidable and in principle contain no unknown parameters. For the moment, however, they need to be fitted to present data because of large uncertainties in the ratio of $KK\pi$ and $\eta\pi\pi$ decays of $\eta(1440)$, which we now discuss. The BES collaboration [34] has recently determined branching ratios of $\eta(1440)$ to $KK^*(890)$, KK_0 and $\eta\pi\pi$; we fit the relative contributions between $\eta\sigma$ and $a_0(980)\pi$ to the $\eta\pi\pi$ channel to the present data. The BES fit shows that the dominant decay channel is $KK^*(890)$. The small contribution from KK_0 has an error approaching 100% of its magnitude. According to the BES work, the $\eta\pi\pi$ decay is weak: 10–20% of $K\bar{K}\pi$. Similar ratios are to be found in the work of Mark III [27] and DM2 [28]. The magnitudes of triangle diagrams fitted here correspond to an intensity ratio $KK\pi/\eta\pi\pi = 7$, in satisfactory agreement with the BES determination. In contrast, data on $\bar{p}p \to \eta(1440)\sigma$ have been used in Ref. [3] to deduce the ratio

$$\frac{BR[\eta(1440) \to KK\pi]}{BR[\eta(1440) \to \eta\pi\pi]} = 0.61 \pm 0.19. \tag{22}$$

The large discrepancy between these two sources of data needs comment. The $\eta(1440)\sigma$ channel is suppressed in $\bar{p}p$ annihilation at high $\eta\pi\pi$ masses by the limited phase space available to the spectator σ; its amplitude goes to zero for low σ mass because of the Adler zero in the $\pi\pi$ amplitude. There is a second suppression factor at high $\eta\pi\pi$ masses. For the 2-body process $\bar{p}p \to \eta(1440)\sigma$, there is a phase space factor k, where k is the momentum of the $\eta(1440)$ in the $\bar{p}p$ rest frame. The suppression caused by these two factors is illustrated in Fig. 3(b) of Ref. [34]. The surviving $\eta(1440)$ signal is attenuated by a factor 3 between $\eta\pi\pi$ masses of 1410 and 1465 MeV. This is just the mass region where the KK^* decay of $\eta(1440)$ is rising rapidly. A final uncertainty concerns interferences between $\eta(1440)$ and the broad $\eta(2190)$; these were ignored in deriving equn. (22) but may be important. Thus the present situation concerning this ratio is confused.

From Table 2, the branching fraction of $\eta(1440)$ decaying directly to $a_0(980)\pi$ is $0.4\times$ that for decays to $\eta\sigma$. Allowing for additional contributions via triangle graphs, the overall ratio

$$\frac{BR[\eta(1440) \to \eta\sigma]}{BR[\eta(1440) \to a_0(980)\pi]} = 1.1 \pm 0.15. \tag{23}$$

This compares quite well with the value obtained in Ref. [3] of $0.78 \pm 0.12 \pm 0.10$.

With the inclusion of the triangle graphs, the contribution from $\eta(2190)$ is not well determined. The reason is that this broad signal is easily confused with that from $\eta\sigma$ contributions produced via triangle graphs from $\eta(1440)$ initial states, and particularly $\eta\sigma$ contributions arising via rescattering from $\eta(1295)$.

The contribution from $\eta(1295)$ is particularly poorly determined. In the absence of triangle graphs, Table 2 estimates it to be 2.8%. With triangle graphs included, it could lie anywhere in the range 0 to 10%. It is somewhat surprising that it makes a smaller contribution than $\eta(1440)$, which, from its strong KK^* decay, appears likely to be the radial excitation of $\eta'(958)$. A natural explanation, advanced in Ref. [33], is that the $\eta(2190)$ is a glueball state and mixes with $\eta(1440)$; the $\eta(1440)$ can then be produced preferentially via its glueball component.

In summary, triangle graphs undoubtedly make significant contributions to decays of $\eta(1440)$. They explain naturally the essential but curious features of the Dalitz plot. A full quantitative understanding requires a combined fit to data from both $\bar{p}p$ annihilation and J/Ψ radiative decays to both $\eta\pi\pi$ and $K\bar{K}\pi$ channels.

5.1 $\eta(1440) \to f_0(975)\eta$

We have recently reported evidence for a threshold enhancement in $f_0(975)\eta$ with quantum numbers $J^P = 0^-$ [42]. As a test, the decay $\eta(1440) \to f_0(975)\eta$ has been added to the present analysis. It gives a small but barely significant improvement in log likelihood, and the fit becomes less stable because of cross-talk with the decay $\eta(1440) \to \eta\sigma$. The decay to $f_0(975)\eta$ is likely to be suppressed strongly in data at rest by the small phase space available for production of the high mass side of the $f_0(1440)$.

6 Summary

The essential points which have emerged from this analysis are:

– The $\eta(1440)$ is definitely present, but probably with large interferences with $\eta(2190)$; there is maximal destructive interference between $a_0(980)\pi$ and $\eta\sigma$ decay modes.
– There is no definite evidence for the presence of $\eta(1295)$. However, when triangle graphs are included in the analysis, a contribution up to 10% could be accomodated. Its small magnitude compared to $\eta(1440)$ is noteworthy.
– The $f_0(1370)$ is confirmed with $\Gamma(4\pi)/\Gamma(2\pi) \geq 5$. Within the limited phase space available for present data, $BR[f_0(1370) \to \rho\rho]/BR[f_0(1370) \to \sigma\sigma] = 0.98 \pm 0.25$.

7 Acknowledgement

We thank the Crystal Barrel group for the use of the data. We wish to thank the technical staff of the LEAR machine group and of all the participating institutions for their invaluable contributions to the success of the experiment. We acknowledge financial support from the British Particle Physics and Astronomy Research Council (PPARC). The St. Petersburg group acknowledges gratefully financial support from PPARC and INTAS grant 95-263.

References

[1] P. Baillon et al., Nu. Cim. 50A (1967) 393.

[2] D.L. Scharre et al., Phys. Lett. B97 (1980) 329.

[3] A. Amsler et al., Phys. Lett. B358 (1995) 389.

[4] A. Abele et al., Nucl. Phys. B. B514 (1998) 45.

[5] Particle Data Group, Euro. Phys. Jour. C3 (1998) 1.

[6] V.A. Polychronakos et al., Phys. Rev. D19 (1979) 1317; A.D. Martin and E.N. Ozmutlu, Nucl. Phys. B158 (1979) 520.

[7] D. Cohen et al., Phys. Rev. D22 (1980) 2595.

[8] A. Etkin et al., Phys. Rev. D25 (1982) 1786.

[9] B. Hyams et al., Nucl. Phys. B64 (1973) 134; G. Grayer et al., Nucl. Phys. B75 (1974) 189; W. Ochs, Ph. D. thesis, University of Munich (1973).

[10] C. Amsler et al., Phys. Lett. B291 (1992) 347.

[11] V.V. Anisovich et al., Phys. Lett. B323 (1994) 233.

[12] D.V. Bugg, A.V. Sarantsev and B.S. Zou, Nucl. Phys. B471 (1996) 59.

[13] U. Thoma, *Hadron Spectroscopy* , AIP Conf. Proc.432 (1998) 322.

[14] A. Bettini et al., Nu. Cim. 42A (1966) 695.

[15] C. Amsler et al., Phys. Lett. B322 (1994) 431.

[16] M. Gaspero, Nucl. Phys. A562 (1993) 407.

[17] A. Adamo et al., Nucl. Phys. A558 (1993) 13C.

[18] A. Bertin et al., Phys. Rev. D57 (1998) 55.

[19] D. Barberis et al., Phys. Lett. B413 (1997) 217, B453 (1999) 316 and 325 and B462 (1999) 462;

[20] D. Barberis et al., Phys. Lett. B. 471 (2000) 440.

[21] C. Amsler et al., Phys. Lett. B355 (1995) 425.

[22] A. Abele et al., Nucl. Phys. A609(1996) 562.

[23] D.V. Bugg et al., Phys. Lett. B353 (1995) 378.

[24] A. Abele et al., Phys. Lett. B380 (1996) 453.

[25] N.N. Achasov and G.N. Shestakov, Phys. Rev. D

[26] J.Z. Bai et al., Phys. Lett. B440 (1993) 217.

[27] J.Z. Bai et al., Phys. Rev. Lett. 65 (1990) 2507.

[28] J.-E. Augustin et al., Phys. Rev. D46 (1992) 1951.

[29] E. Aker et al., Nucl. Instr and Methods A321 (1992) 69.

[30] R. Bizzari et al., Nucl. Phys. B14 (1969) 169.

[31] B.S. Zou and D.V. Bugg, Phys. Rev. D48 (1993) 3948.

[32] D.V. Bugg et al., Phys. Rev. D50 (1994) 4412.

[33] D.V. Bugg. L. Y. Dong and B.S. Zou, Phys. Lett. B458 (1999) 511.

[34] J.Z. Bai et al., Phys. Lett. B440 (1998) 217.

[35] A. Bertin et al., Phys. Lett. B361 (1995) 187 and B400 (1997) 226; C. Cicalo et al., Phy. Lett. B462 (1999) 453.

[36] J. Chen, X.-Q.Li and B.S. Zou et al., hep-ph/0001004 (2000).

[37] P. Minkowski and W. Ochs, Frascati Physics Series 15, eds. T. Bressani, A. Feliciello and A. Filippi, (1999) 245.

[38] A. Abele et al., Phys. Lett. B423 (1998) 175.

[39] V.V. Anisovich and A.V. Sarantsev, Phys. Lett. B382 (1996) 429; V.V. Anisovich et al., hep-ph/9711319, Phys. of Atomic Nuclei (in press).

[40] D. Aston et al., Nucl. Phys. B296 (1988) 493.

[41] V.V. Anisovich and A.A. Ansel'm, Sov. Phys. Usp 88 (1966) 117.

[42] A.V. Anisovich et al., Phys. Lett. B472 (2000) 168.

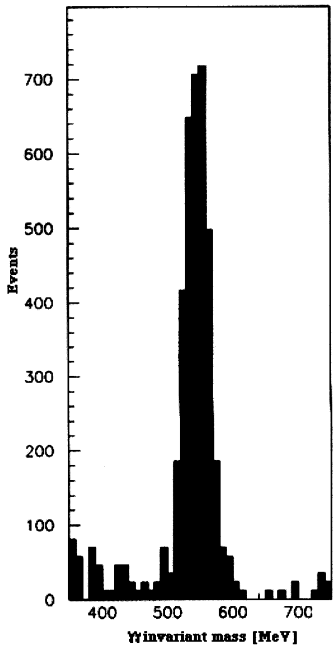

Fig. 1. The $\gamma\gamma$ mass spectrum from events failing to fit reaction (2).

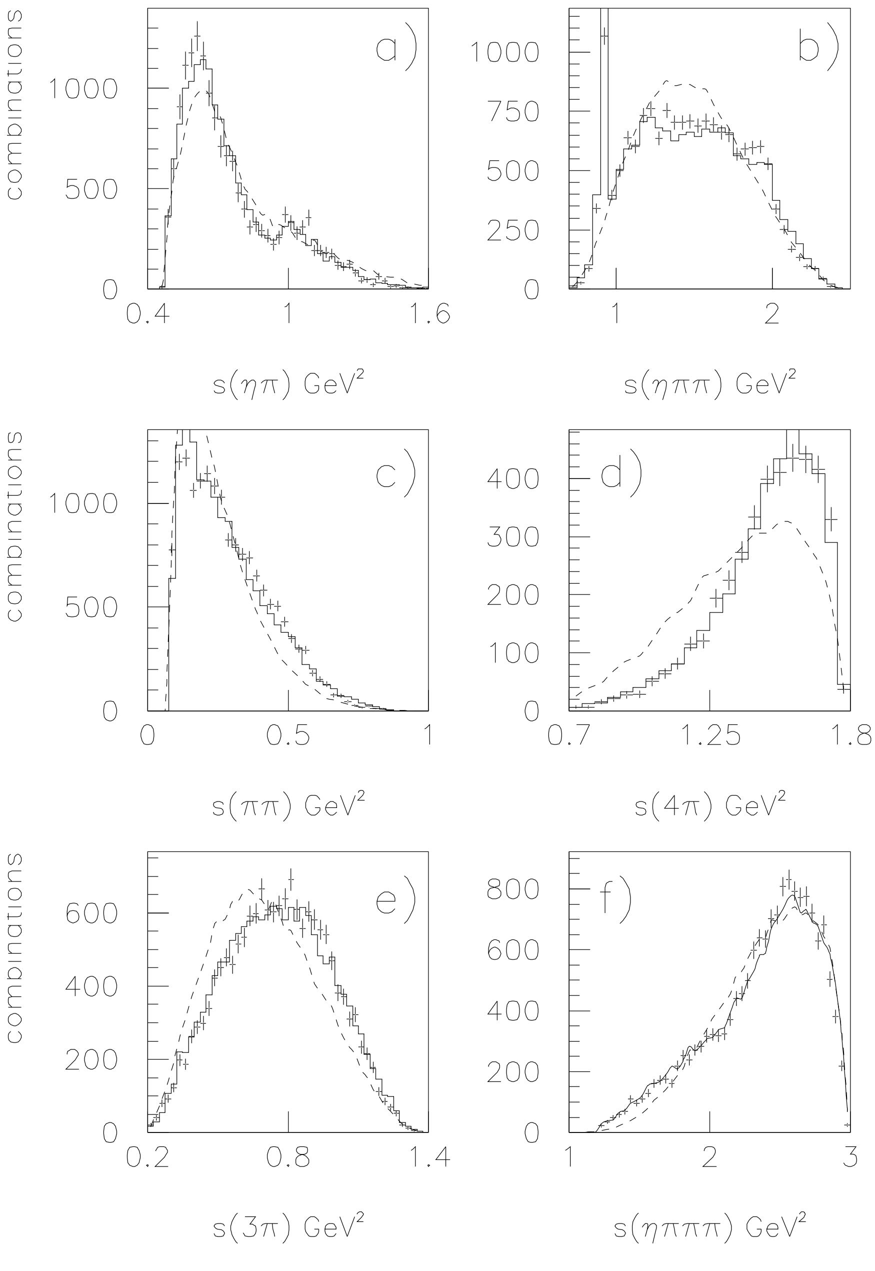

Fig. 2. Projections on to (a) $s(\eta\pi)$, (b) $s(\eta\pi^+\pi^-)$, (c) $s(\pi^+\pi^-)$, (d) $s(4\pi)$, (e) $s(3\pi)$ and (f) $s(\eta 3\pi)$. Histograms show the fit; phase space is shown by the dashed curves.

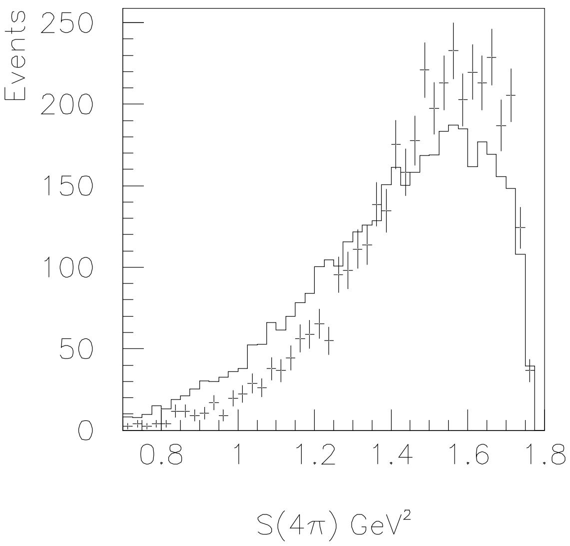

Fig. 3. Comparison of the projection on to $s(4\pi)$ with the fit (shown by the histogram) omitting $f_0(1370)$.

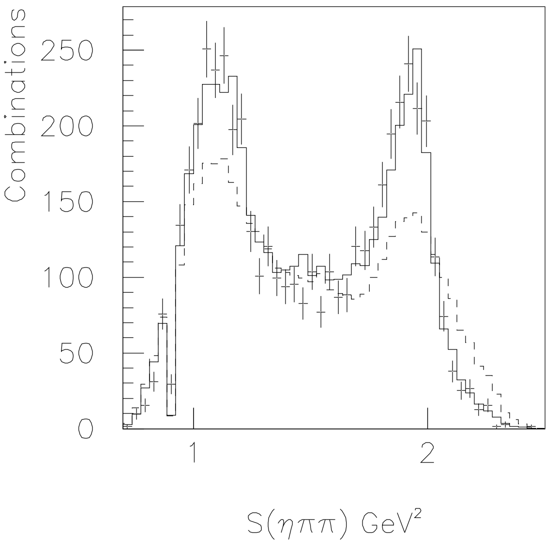

Fig. 4. Comparison of the best fit (full histogram) with asymmetric pairs of pions, selected with R_{13} or R_{14} $<$ 0.6 or $>$ 1/0.6. The dashed histogram shows phase space. Any events containing an $\eta'(958)$ have been rejected as described in the text.

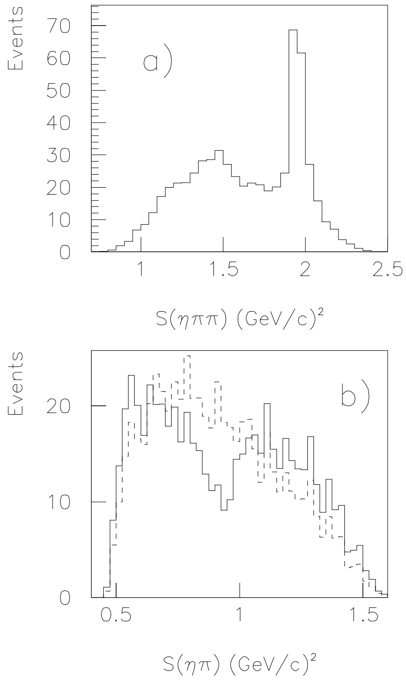

Fig. 5. (a) Projection of the fit (with Monte Carlo statistics) on to $s(\eta\pi^+\pi^-)$ from one charge combination of $\eta(1295)$, $\eta(1440)$ and $\eta(2190)$; (b) projection on to $s(\eta\pi)$ from one charge combination of the fitted $\eta(1440)$; the full line shows the contribution including both decay modes of $\eta(1440)$ and the dashed line the contribution from $\eta\sigma$ alone.

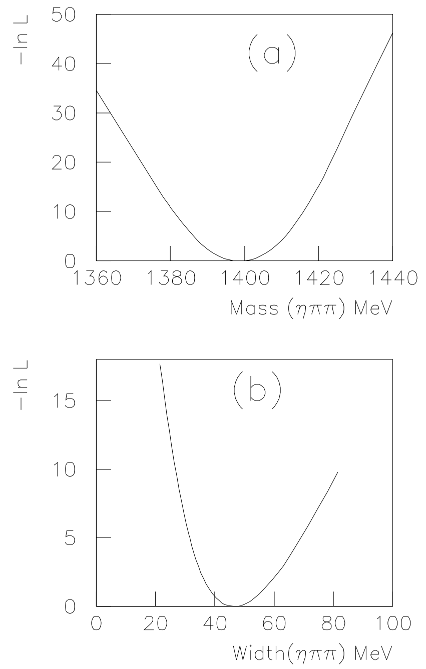

Fig. 6. Log likelihood v. (a) $M[\eta(1440)]$, and (b) $\Gamma[\eta(1440)]$.

Fig. 7. The $\pi\pi$ S-wave amplitude f_0 in $\bar{p}p \to \eta f_0$, reproduced from Ref. 22.

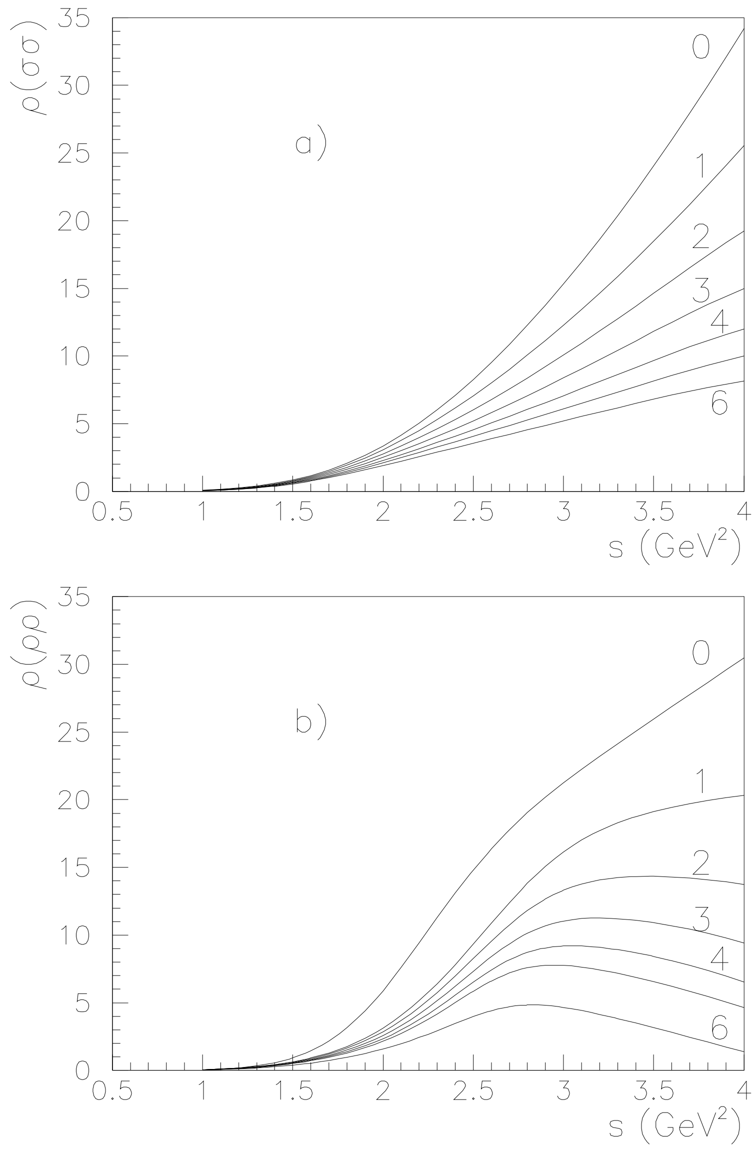

Fig. 8. The phase space for (a) $\sigma\sigma$, (b) $\rho\rho$ for values of α in the form factor from 0 to 6 GeV^{-2}.

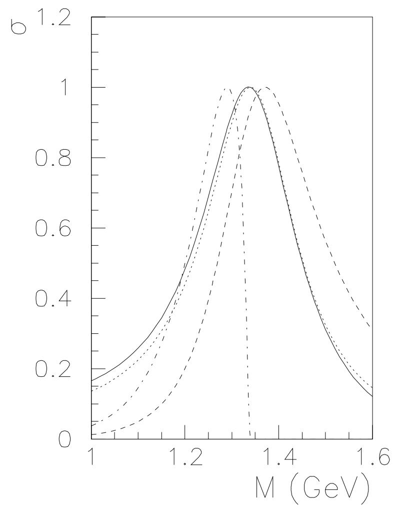

Fig. 9. The shape of $f_0(1370)$: full curve in the 2π channel, dashed curve in the 4π channel; dot-dashed curve as it appears in the 4π channel with the phase space available in $\bar{p}p \to \eta f_0$; the dotted curve shows a Breit-Wigner resonance of constant width centred at the same mass as the 2π curve.

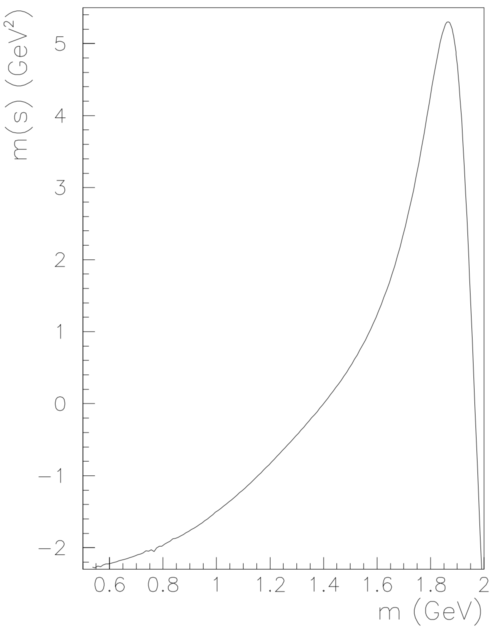

Fig. 10. The dispersive correction $m(s)$ to the mass.

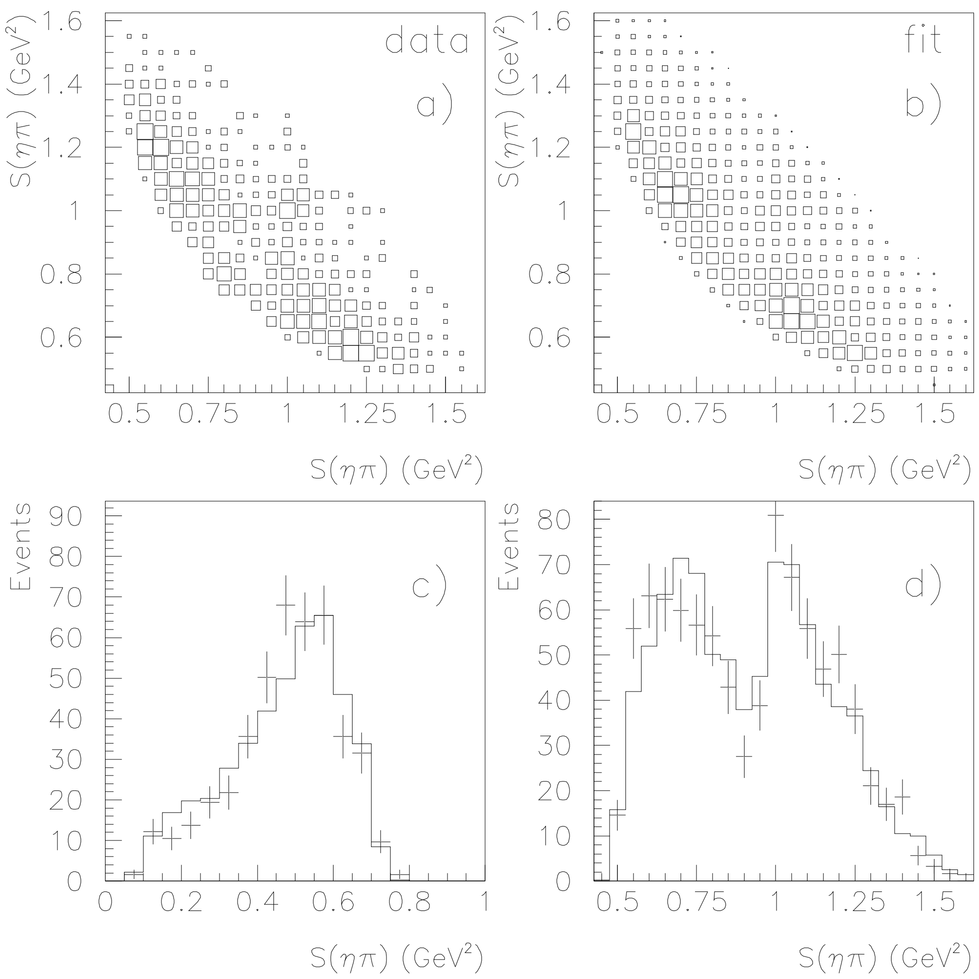

Fig. 11. (a) Dalitz plot for $\eta\pi^+\pi^-$ events selected in the region of mass 1382 to 1422 MeV by the R cut described in the text; (b) the fit including triangle graphs; (c) projection on to $s(\eta\pi)$, (d) projection on to $s(\pi^+\pi^-)$. In (c) and (d), points with error bars are data and histograms show the maximum likelihood fit.

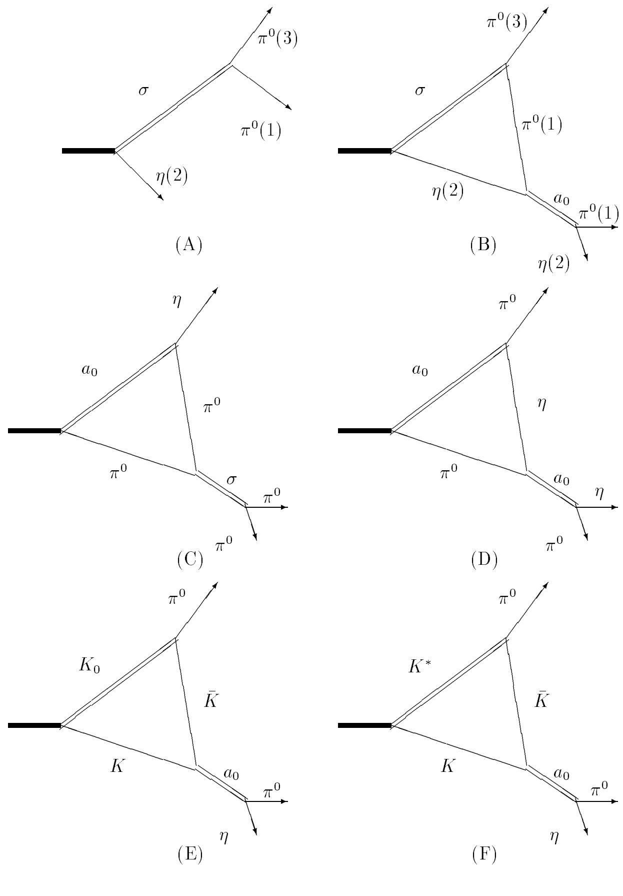

Fig. 12. (a) The amplitude for the bare $\eta\sigma$ amplitude; (b)–(f) triangle diagrams for decays of $\eta(1440)$ to $\eta\pi\pi$ final states.

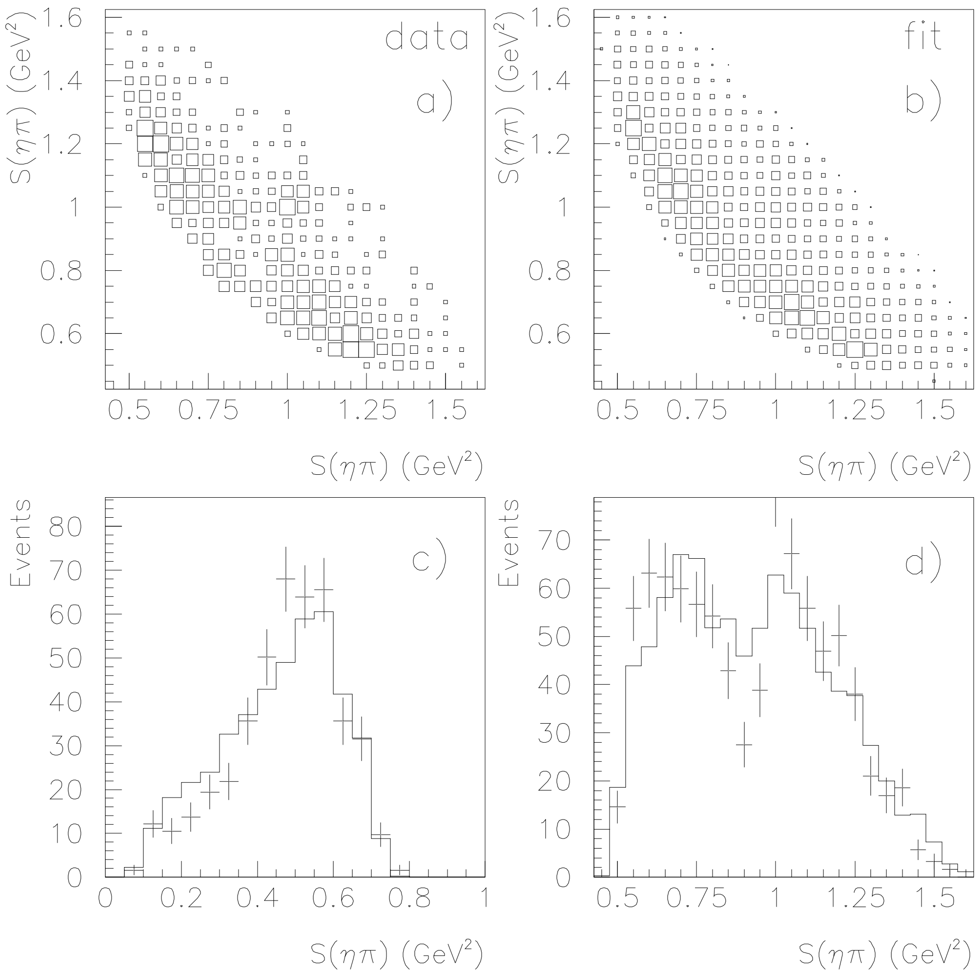

Fig. 13. As Fig. 11, the best fit excluding all triangle graphs.

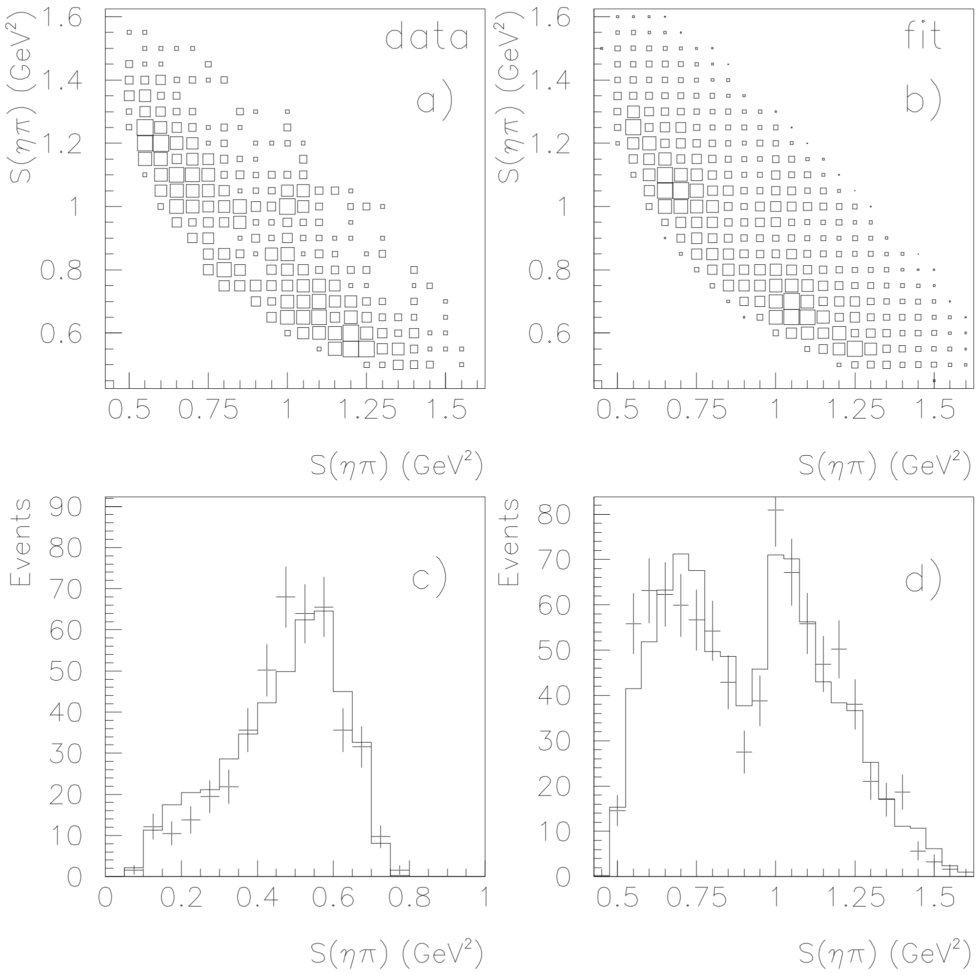

Fig. 14. As Fig. 11, keeping only the triangle graphs of Figs. 12(e) and (f).